Kinetics of Nitric Acid Uptake by Salt

ARTICLE *in* THE JOURNAL OF PHYSICAL CHEMISTRY · SEPTEMBER 1994

Impact Factor: 2.78 · DOI: 10.1021/j100090a014

3 AUTHORS:

Frederick Frank Fenter
Frontiers Publishing
27 PUBLICATIONS **678** CITATIONS
SEE PROFILE

Francois Caloz
Diamoond SA
21 PUBLICATIONS **491** CITATIONS
SEE PROFILE

Michel J Rossi
Paul Scherrer Institut
259 PUBLICATIONS **6,612** CITATIONS
SEE PROFILE

Kinetics of Nitric Acid Uptake by Salt

Frederick F. Fenter, François Caloz, and Michel J. Rossi*

Laboratory for Air and Soil Pollution (L.P.A.S.), Swiss Federal Institute of Technology, CH-1015 Lausanne, Switzerland

Received: April 14, 1994; In Final Form: July 11, 1994®

The kinetics of the uptake of HNO_3 on a series of salt powders (NaCl, NaBr, KCl, and KBr) has been studied in a Teflon-coated, low-pressure flow reactor. HCl and HBr are found to be the sole products of the reactions, and, within experimental uncertainty, all the HNO_3 taken up by the salt is converted to HCl or HBr. Values for the uptake coefficients are derived from two experimental procedures: (1) Steady-state uptake of constant HNO_3 flows and (2) real-time monitoring of pulsed quantities of HNO_3. The two procedures yield values in good agreement, and it has been determined that all the salts studied, including the nonreactive $NaNO_3$, are characterized by the same value of the uptake coefficient: $\gamma = (2.8 \pm 0.3) \times 10^{-2}$. A discussion is given for the non-negligible affinity of HNO_3 for the Teflon-coated walls and how this effect is taken into account in our experiments. We develop a model of the uptake kinetics, based on our experimental results, that reproduces the observations over a broad range of experimental conditions. In addition, the uptake of HCl ($\gamma = 3 \times 10^{-2}$) and H_2O ($\gamma < 2 \times 10^{-4}$) on NaCl powder is determined in ancillary experiments. The results may hold implications for the understanding of chloride displacement in marine aerosols.

Introduction

The oxides of nitrogen, including nitric acid, nitric acid anhydride (N_2O_5), and nitrogen dioxide, can react with salt-containing aerosols in the atmosphere to produce gas-phase chlorine-containing species.[1] The issues of the chemical nature, the strength, and the oxidative potential of the chlorine source in the troposphere are far from resolved;[2-7] laboratory experiments,[8-15] atmospheric models[2-5] and in-situ measurements[5] have been designed to address the many facets of the problem, including the role played by the reactions that can occur between nitrogen oxides and sea-salt aerosols. In summary, HNO_3 has been proposed to react with sea-salt aerosols to liberate chlorine in the form of HCl.[15-24] A subsequent reaction between OH radicals and HCl, in one scenario,[2] represents the largest source of free-chlorine atoms in the marine troposphere. The reactions of N_2O_5 and NO_2 with NaCl may provide an additional source of Cl atoms;[1,5,6,8-14] the products, $ClNO_2$ and ClNO, are readily photolyzed by sunlight, providing a potential direct source of Cl atoms, or hydrolyzed to yield HCl. Studies of the kinetics of the last two reactions are under way in several laboratories to assess their role in the oxidative potential of the marine troposphere.

The reaction of HNO_3 with NaCl has been the subject of several studies. In the early 1960s, Cadle and Robbins reported an immeasurably fast reaction between NO_2 and NaCl in the presence of water vapor in an aerosol reactor;[15] they attributed the observed HCl formation to the reaction of nitric acid (formed by hydrolysis of NO_2) with the salt. Since 1955, atmospheric aerosol measurements have revealed a deficit in chloride content,[16,22,24,25] which has been rationalized by the reaction of nitric acid with sodium chloride. On the basis of a simple thermodynamic model, Brimblecombe and Clegg concluded that HCl should be displaced by HNO_3 in these aerosols.[18,19] Mamane and co-workers focused on the transformation of salt grains by exposure to nitric acid and other nitrogen oxides, finding that the nitrate which forms is located on the surface of the solid.[20,21,23] In more recent laboratory studies, Finlayson-Pitts et al. exposed salt samples of N_2O_5 with a nitric acid impurity;[13] the HCl product they observed was attributed to the reaction between nitric acid and sodium chloride. Unlike the NO_2 and N_2O_5 reactions with NaCl, there is no previous kinetic study of the corresponding HNO_3 reaction. In fact, even crude bulk experiments to determine an approximate value for the uptake coefficient, γ, have not yet been carried out for this reaction of certain atmospheric importance; even stratospheric modelers have expressed an interest in this measurement because of the large amounts of NaCl that can be injected into the middle atmosphere by volcanic eruptions.[26]

In this paper, we report experiments conducted in a low-pressure flow reactor (Knudsen cell) designed to isolate and elucidate the kinetics of the HNO_3 reactions with a series of salt powders:

$$HNO_3 + NaCl \rightarrow NaNO_3 + HCl \quad \Delta H°(298) = -13.95 \text{ kJ/mol} \quad \text{(R1)}$$

$$HNO_3 + KCl \rightarrow KNO_3 + HCl \quad \Delta H°(298) = -15.13 \text{ kJ/mol} \quad \text{(R2)}$$

$$HNO_3 + NaBr \rightarrow NaNO_3 + HBr \quad \Delta H°(298) = -8.13 \text{ kJ/mol} \quad \text{(R3)}$$

$$HNO_3 + KBr \rightarrow KNO_3 + HBr \quad \Delta H°(298) = -2.18 \text{ kJ/mol} \quad \text{(R4)}$$

By using a variety of techniques and initial conditions, coupled with a kinetic simulation of the overall process, we can calculate a value for the uptake coefficient and, in addition, gain insight into the fundamental kinetic processes of the adsorption and subsequent reaction. Also, we show how experiments conducted with a nonreactive salt sample, $NaNO_3$, can yield insight into the physical chemistry of the adsorption process.

Experimental Details

The study was carried out by using a low-pressure flow reactor shown schematically in Figure 1. The basic consider-

* Author to whom correspondence should be addressed.
® Abstract published in *Advance ACS Abstracts,* September 1, 1994.

0022-3654/94/2098-9801$04.50/0

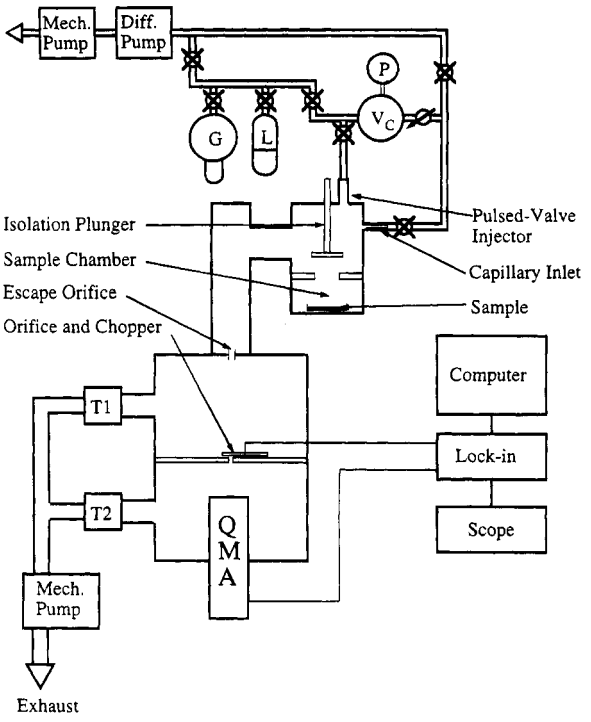

Figure 1. Schematic diagram of the experimental apparatus. G, gas sample; L, liquid sample; P, pressure gauge; V_c, calibrated volume; T1, T2, Turbomolecular pumps; QMA, quandrupole mass analyzer; isolation of the salt sample for control experiments is achieved by use of the isolation plunger.

ations for the use of these reactors has been described in detail previously.[27,28] In summary, the flow rate and the aperture size of the reactor can be chosen to control the densities and residence times of the species in the cell. Total pressure is kept low enough to ensure that the reactor remains in the molecular flow regime.

The cell shown in Figure 1 has been coated with Teflon to minimize the loss of gas-phase species to the walls by adsorption or reaction. It is equipped with two types of entry ports, one a short capillary tube for introduction of the HNO_3 for flowing-gas experiments, the second a wide (1.5 cm) port to which a pulsed valve has been mounted. The cell has two chambers which can be separated with an O-ring sealed plunger to allow for isolation of the solid salt samples during control experiments. The volume of the sample chamber represents 30% of the total volume of the reactor. The escape aperture can be varied by lowering plunger-mounted pin holes onto the permanent aperture. The pulsed valve was supplied by General Valve (Series 9, $\phi = 2$ mm) and was used with a Teflon poppet to minimize potential heterogeneous reactions; in addition, the internal exposed surfaces of the valve were coated with halocarbon wax (Halocarbon Wax Series 1500).

The Knudsen cell is positioned on a vacuum chamber evacuated by turbo-molecular pumps. The effusive beam which is formed at the exit hole of the cell is chopped by a tuning fork at 145 Hz before passing into the ionization volume of a quadrapole mass spectrometer (Balzers model QMG 421) mounted in the second stage of differentially pumped vacuum chamber. The modulated electron-multiplier signal is processed by a lock-in amplifier (Stanford Research SRS 510) and subsequently stored in a digital storage oscilloscope or a digital $x-y$ recorder before transfer of the data to a computer for storage and analysis. The use of the lock-in amplifier is essential for the study of nitrogen oxides such as HNO_3 because of the non-negligible background signal created by the acid and its degradation products as they desorb from the steel walls of the vacuum chamber. Vacuum-chamber sources that can contribute to the signal are eliminated by the phase-sensitive detection.

The solid salt samples were prepared by grinding crystalline salt into powder with a "Wig-L-Bug" amalgamator (Crescent Dental MFG., Co., Chicago, IL). The typical grain size of the samples thus produced, determined by scanning electron microscopy, was found to vary greatly as a function of the milling conditions; typical grain size varied between 5 and 100 μm. We did not attempt to characterize the total internal surface area of our samples because, as discussed below, the initial rate of uptake depends on the geometric area of the sample (10.8 cm^2) and not on the internal surface area of the powder. The salt samples were dried by leaving the powders in the evacuated Knudsen cell at pressures of about 10^{-8} mbar for many hours before the experiment; in addition, the samples were often heated by irradiating the sample dish with a heat lamp.

Nitric acid was prepared by distillation of a 65% solution in water. The purity of the gaseous nitric acid sample was routinely checked by measuring the ratio of the *m/e* 30 to *m/e* 46 signals. This allows the purity to be assessed before an experiment to eliminate possible secondary chemistry involving NO_2 (a potential degradation product) and to ensure that the *m/e* 46 signal is due uniquely to the presence of HNO_3 in the effusive beam. HNO_3 can be unambiguously monitored at *m/e* 63, but the *m/e* 46 signal is about a factor of 20 more intense, which allows experiments to be conducted with smaller flows of HNO_3 (for the same signal-to-noise ratio).

Small amounts of pure HCl were obtained by dripping 96% sulfuric acid onto NaCl powder under vacuum and collecting the HCl that evolved in a trap cooled with liquid nitrogen. HBr was obtained by dripping molecular bromine onto liquid tetralin under dry nitrogen and passing the evolving gases through a trap containing tetralin (to eliminate any traces of molecular bromine) before collecting the HBr in a trap cooled with liquid nitrogen. The purity of the HCl and HBr thus obtained was verified by mass spectrometry.

The gas-phase densities in the Knudsen cell are determined by mass-flow calibrations. These are carried out by monitoring the pressure drop in a small calibrated volume (about 40 cm^3) located between the vacuum line and the flow inlet of the cell. The pressure is monitored by a 0−100-mbar Baratron (absolute pressure transducer). The mass-spectrometer signal is thus characterized as a function of the pressure change (dp/dt), which can be related to mass flow. This procedure is carried out for all the gas-phase reactants and products (HNO_3, HCl, HBr).

The kinetic meter of the Knudsen cell is the escape-rate constant, hereafter referred to as k_{esc}; this quantity is the first-order rate constant for the loss of a gas-phase species in the cell by passage through the aperture. The residence time and density of a gas-phase species are directly related to the value of k_{esc}, and the rate of reactive loss to the salt surface is determined by kinetic competition with the rate of escape; it is therefore necessary to have a precise measurement of this parameter. For this study, we conducted experiments with aperture sizes representing a factor-of-10 variation in k_{esc}. The value of k_{esc} associated with an aperture size is determined experimentally by either (1) abruptly stopping the flow of a gas into the cell at the inlet and following the first-order disappearance of that species or (2) pulsing the gas into the cell via the pulsed valve inlet and monitoring the same first-order decay. In principle, the value is independent of the admission scheme and should scale with the mass as $M^{-0.5}$ (as given by elementary gas-kinetic theory). Deviations from this relation are apparent for nitric acid and are consistent with the hypothesis that nitric acid has some non-negligible affinity for

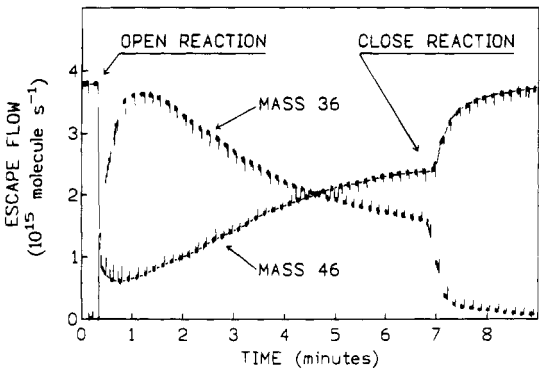

Figure 2. Typical results for a large-flow large-aperture exposure of HNO_3 onto NaCl powder. The HNO_3 uptake (followed at mass 46) and the HCl production (followed at mass 36) are seen to pass through a maximum after about 1 min of exposure. Integration of the HNO_3 consumption and the HCl production allows the calculation of the yield (see text). At the closing of the isolation plunger, the initial steady-state concentration of HNO_3 in the cell is re-established. A dashed line has been drawn through the *m/e* 46 data for the sake of clarity.

TABLE 1: Knudsen Cell and MS Parameters

cell parameter	value
volume	960 cm^3
surface area (total)	1200 cm^2
surface area of sample	10.8 cm^2
number density, cm^{-3}	$(0.1-100) \times 10^{11}$
surface collision frequency	$3.80(T/M)^{0.5}$ s^{-1} cm^{-2}
"large" escape aperture diameter	≈3 mm
"small" escape aperture diameter	≈1 mm
"large" escape rate constant	$0.31(T/M)^{0.5}$ s^{-1}
"small" escape rate constant	$0.045(T/M)^{0.5}$ s^{-1}

the Teflon surfaces of the reactor walls. We discuss this observation in detail below. The parameters for the Knudsen cell reactor used in this study are presented in Table 1.

Two types of experiments are carried out. The first, referred to here as steady-state experiments, are conducted by (1) isolating the salt sample (prepared as described above) in the lower chamber of the reactor, (2) flowing nitric acid through the larger upper volume of the reactor until a steady state is achieved, (3) opening the lower chamber while monitoring one or several masses with the detector to follow the uptake of nitric acid by the surface and the production of the hydrohalogenic acid, and (4) closing the lower chamber to terminate the reaction and to observe the reestablishment of the initial steady-state flow of nitric acid. Typical reaction cycles for steady-state experiments are shown in Figures 2 and 3. This basic procedure can be altered to gain additional insight into the overall chemical process, examples of which are presented in the Results.

A second procedure is employed for the pulsed-valve introduction of nitric acid into the cell. For these experiments, the nitric acid is pulsed into the cell first with the sample chamber closed, from which a value for k_{esc} can be determined. A second pulse is injected with the sample chamber open to obtain a decay trace of the nitric acid signal in the presence of the sample. The size of the HNO_3 pulse is selected by adjusting the pressure behind the valve and by selecting the duration of the open state. In this way, pulses can be prepared that are both small (on the order of 10^{14} molecules/pulse) and reproducible (to within 5%). Because of the low doses and fast signal rise-times involved in these experiments, we record the electron multiplier signal directly without lock-in amplification. In Figure 4, we show the result of a typical pulsed-valve experiment.

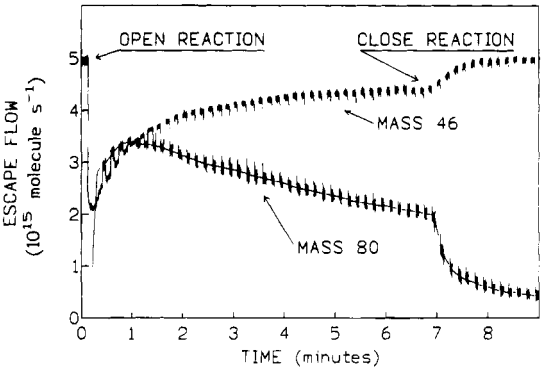

Figure 3. Typical results for the large-flow large-aperture exposure of HNO_3 to NaBr powder. HNO_3 (mass 46) uptake rapidly saturates after the start of the experiment, and the production of HBr (mass 80) is shifted to slightly longer times (relative to uptake) compared to the chloride exposed to similar flows of nitric acid in Figure 2. A dashed line has been drawn through the *m/e* 80 data for the sake of clarity.

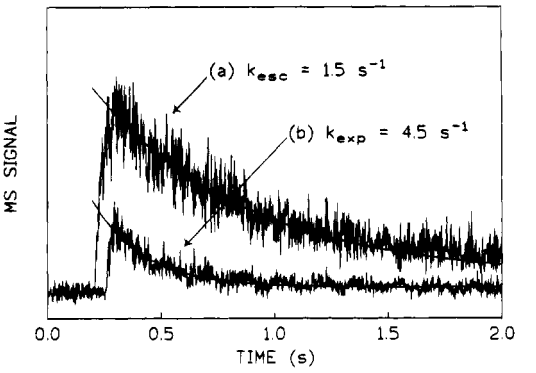

Figure 4. Real-time monitoring of the *m/e* 46 signal after pulsed valve injection of HNO_3 (large apeture). Pulses contain ~10^{14} molecules HNO_3: (a) small-volume escape rate determined with the $NaNO_3$ sample isolated. The value of k_{esc} is 50% faster than the value calculated from the gas-kinetic expression in Table 1. (b) The experimental trace (mass 46) in the presence of the $NaNO_3$ powder fit by a simple exponential decay function.

Results

This section is divided into four parts. The first describes the experiments from which the products of the reactions are determined, the second considers the observed variation in the k_{esc} values, the third discusses results of the uptake experiments carried out in the limit of small doses, and the fourth presents the results of experiments carried out under a wide range of initial conditions.

A. Product Spectra and Yields. In a first series of experiments, the mass spectrum of the products of reaction (1) is characterized to confirm the conclusion of previous studies that HCl is the sole product of the reaction. These experiments are conducted in the steady-state mode, and a mass spectrum is registered before and during nitric acid exposure to the salt powder. Examples of spectra are shown in Figure 5, where it can be seen that upon reaction, there is a decrease in the gas-phase density of nitric acid and a production of HCl. In a separate experiment, the sensitivities of the mass-spectrometric detection are determined for HCl and for HNO_3 by mass-flow calibration. From integration of experimental traces like that shown in Figures 2, we determine that that the yield of HCl is (115 ± 25)% relative to the KNO_3 taken up by the sample. The uncertainty is estimated from the systematic errors associated with the mass-flow calibrations, whose precision is limited by the affinity of these species for the reactor walls. From similar experiments conducted on the bromide samples, the sole

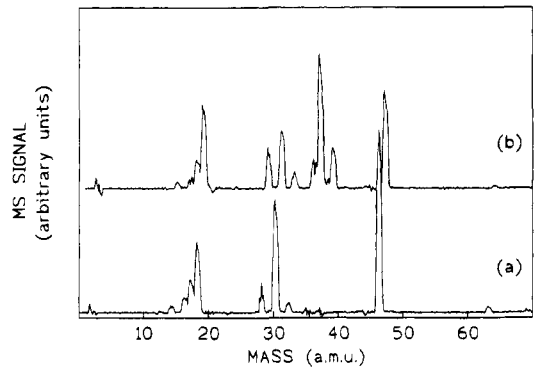

Figure 5. Mass spectra recorded (a) before and (b) during reaction with solid NaCl powder (large aperture, lock-in amplified). The reduction of HNO_3 signals at *m/e* 17, 30, 46, and 63 is evident, as well as the appearance of the HCl peaks at *m/e* 35−38. Other peaks are due to the background gases H_2O, N_2, and O_2. The second spectrum is offset vertically and by one *m/e* unit for the sake of clarity.

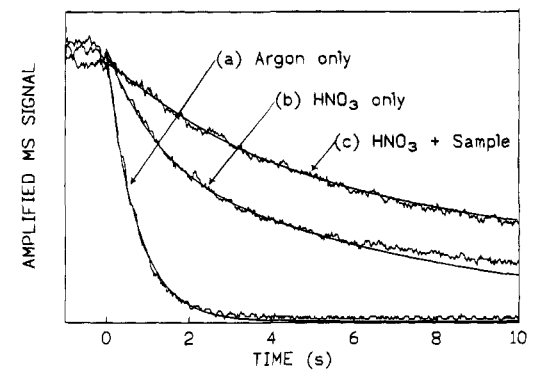

Figure 6. Escape flow of Ar and HNO_3 from the reactor after turning off the inlet flow (large aperture): (a) The argon signal decay at mass 40 is a simple exponential with the rate constant given by the gas-kinetic expression of Table 1. (b) HNO_3 escape flow (signal at mass 46) does not obey simple exponential decay and is fitted by eq 3. (c) The escape flow of HNO_3 (mass 46) in the presence of the degassing, saturated $NaNO_3$ sample. A net rate of desorption can be estimated by using eq 13. For experiments b and c, the stopped initial flow = 3.5×10^{15} molecules s^{-1}.

new species in the product spectrum is found to be HBr. In particular, no signal at *m/e* 158, 160, and 162 is observed, which would correspond to the formation of molecular bromine. With a mass-flow calibration for HBr, we can calculate the mass balance for the bromide reactions; from the integration of the calibrated traces shown in Figure 3, we find that the yield is (80 ± 25)%. The potential less-than-unity yield may be due to the slower processing of the HNO_3 by bromides, and there may be a quantity of HBr product that is not observed due to adsorption to the reactor walls. From experiments like those shown in Figures 2 and 3, it is determined that the appearance of the hydrohalogenic acid was kinetically shifted to longer times for the bromides relative to the chlorides under identical experimental conditions. The sole product of reactions (R-1−4) is the corresponding hydrohalogenic acid (HCl or HBr) and is formed, upon exposure to large doses of nitric acid, with a one-for-one stoichiometry (within experimental uncertainty).

B. Variation of k_{esc}. Before discussing the details of the kinetic results, it is necessary to explain how k_{esc} was determined for the sticky compound HNO_3. Ideally, the value of k_{esc} is a function of the molecular mass of the gas-phase species, as described in Table 1. In our reactor, this relation holds well for "inert" gases such as Ar, He, CO_2, and N_2. In Figure 6, a typical escape-rate decay for argon is shown to be described by a simple exponential decay. The case for HNO_3 is more complex. When HNO_3 is admitted to the cell via a pulse of the solenoid valve, the signal decay is faster than expected based on the k_{esc} calculated by using the expression in Table 1. Conversely, in the steady-state experiments, where the HNO_3 flow is established and subsequently stopped, the signal falls off more slowly than predicted from the gas-kinetic expression of Table 1 and is not well-described by a simple exponential decay function. These observations are understood in terms of HNO_3 adsorption onto and desorption from the Teflon walls of the reactor; i.e., the walls can act as either an additional source or sink of HNO_3 depending on the experimental conditions. Indeed, the affinity of nitric acid for Teflon has been noted in other laboratories; it is, for example, notoriously difficult to detect HNO_3 in Teflon-lined smog chambers.[29,30]

In the pulsed valve experiments, k_{esc} is thus large relative to the ideal value because of an additional loss term of HNO_3 by adsorption onto the previously unexposed reactor walls. The deviation was most apparent with the large orifice configuration, for which the observed k_{esc} was as much as a factor of 2 greater than the scaled gas-kinetic value. The experimentally determined k_{esc} was found to depend on factors such as pulse size, temperature, and time between HNO_3 injections. For all the pulsed valve experiments, we measured k_{esc} for the specific conditions before each experiment and used this value in the derivation of the reactive loss in the subsequent exposure of the salt sample.

The hypothesis of HNO_3 wall affinity offers an explanation for the systematic behaviour of the escape rate for steady-state experiments as well. The apparent slowing of the escape rate is due to the additional source of wall outgassing. Figure 6 (trace B) shows a escape-rate trace for HNO_3 next to the argon result, conducted under identical experimental conditions. In contrast to the argon trace, the HNO_3 signal is not described by simple exponential decay; we fit the trace with a more complicated function that was derived from the hypothesis that the outgassing walls provide an independent source of gas-phase nitric acid. Upon stopping the flow, the rate of change of the number of molecules in the cell can be expressed by

$$dN/dt = -k_{esc}N + f_s(t) \quad (1)$$

where N and $f_s(t)$ represent the gas-phase number of HNO_3 molecules and a wall source function for nitric acid, respectively. We approximate the net wall outgassing to be a source of S_w (molecules s^{-1}) that decays exponentially with the constant k_w:

$$f_s(t) = S_w e^{-(k_w t)} \quad (2)$$

Integration of eq 1 then gives the following expression:

$$N(t) = \frac{S_w}{(k_{esc}-k_w)} e^{-(k_w t)} + \left(\frac{-S_w}{(k_{esc}-k_w)} + \frac{E_{int}}{k_{esc}}\right) e^{-(k_{esc} t)} \quad (3)$$

where F_{int} represents the flow that is turned off at the start of the experiment.

The goal of the exercise is to demonstrate that the data can be fit with a function that uses the true, gas-kinetic value of k_{esc} for nitric acid and that includes a simple additional term to represent the wall outgassing. The kinetics of the wall interaction is certainly more complicated, but the present model is sufficient to lend insight into the process. Equation 3 was fitted by nonlinear least-squares optimization to eight traces representing large-orifice experiments with varied initial flows ($2.7-20.9 \times 10^{14}$ molecule s^{-1}). F_{int} is measured, k_{esc} is set at its gas-kinetic value, and the equation is optimized allowing k_w and S_w to vary. The values returned for the parameters S_w and

k_w are remarkably coherent for the entire group of experiments. The wall source is found to be proportional to the stopped initial flow ($S_w = (0.56 \pm 0.08)F_{int}$) and the exponential decay constant, k_w, is determined to be (0.15 ± 0.02) s^{-1}, where the estimated errors give the $1 - \sigma$ statistical limit of the averages. The qualitative understanding of the wall outgassing is discussed below in conjunction with the determination of the uptake coefficient and the modeling of the uptake kinetics.

C. Low-Dose Experiments. We have two means of observing the kinetics of nitric acid uptake on the salt samples in the limit of low exposure. Small amounts of HNO_3 can be pulsed into the reactor and the subsequent decay observed in real time, or a steady state experiment can be conducted in the low-flow, short-residence-time (large aperture) configuration. We use the term "low exposure" to represent the domain of gas-phase concentrations for which surface saturation effects are not observable. Below, we develop a kinetic model to reproduce the experimental observations taken over a broad range of initial concentrations; in the model the surface uptake is taken to be a second-order process with respect to the gas-phase concentration of nitric acid and the number of surface sites, denoted as S_{surf}:

$$\text{rate of uptake} = k_1 N_{HNO_3} S_{surf} \quad (4)$$

In the low-exposure domain, the value of S_{surf} does not change significantly, and the process can be considered first order with respect to $[HNO_3]$; thus, the reactive uptake can be described by a pseudo-first-order rate constant: $k_{uni} = k_1 S_{surf}$. In this limit of low exposure, the value of k_{uni} is equated to the product of the collisional frequency with the solid surface (ω) with the uptake coefficient (γ); the latter is simply the probability that a collision leads to the loss of the gas-phase species:

$$\gamma = k_{uni}/\omega \quad (5)$$

With the pulsed valve, we introduce small and reproducible quantities of nitric acid into the reactor. For each experiment a set of signals is recorded: First, k_{esc} is measured in the upper volume of the Knudsen cell reactor under the pertinent experimental conditions. Nitric acid is then injected into the cell with the sample chamber open, under otherwise identical conditions, and the corresponding decay of HNO_3 is registered in real time. The production trace of HCl or HBr can be recorded in a subsequent experiment. Typical signals of a pulsed-valve experiment are shown in Figure 4 for the case of HNO_3 uptake on a $NaNO_3$ sample.

The value for k_{uni} is derived by fitting the observed signal change (at *m/e* 46) to exponential decay function and then subtracting the value of the experimentally determined k_{esc} (corrected for the different volumes). To ensure that we are observing low-exposure behavior, the doses introduced by the pulsed valve are kept as small as possible, and, therefore, the decay traces tend to be noisy. The uncertainty associated with an individual determination is on the order of 20%. When the same experiments are carried out with the reactor configured with a smaller aperture (longer residence time with respect to effusive loss from the cell) a value for k_{uni} is derived that is in good agreement with the other experiments. The results of the pulsed-valve experiments are presented in Table 2. It can be seen that there is no systematic difference in uptake among the salts studied. The average of all the pulsed valve experiments (for the 10.8-cm^2 sample dish) is given by $k_{uni} = (2.9 \pm 0.7)$ s^{-1}.

Steady-state experiments can be conducted in the low-dose limit if the residence time in the cell is short (i.e., with the large aperture) and if the gas-phase densities are reduced to a minimum value. Figure 7a shows the rapid establishment of a steady state during one such experiment, for which the flow of nitric acid into the cell is 3.5×10^{14} molecules s^{-1} and for which an orifice with an associated k_{esc} of 0.7 s^{-1} was used. The value for k_{uni} can be derived by applying the steady-state hypothesis for the gas-phase HNO_3 density:

TABLE 2: Results of Low-Dose Experiments

salt	flow, 10^{14} molecules s^{-1}	N_o,[a] 10^{14} molecules	$(S_i/S_f - 1)$[b]	k_{uni},[c] (s^{-1})	expts
		Steady-State Experiments			
NaCl	0.1–42.0	0.1–60.0	3.5 ± 0.5	2.5 ± 0.4	14
KBr	1.7–10.1	2.4–14.4	3.2 ± 0.4	2.2 ± 0.3	3
$NaNO_3$	4.2–18.2	6.0–26.0	3.4 ± 0.7	2.4 ± 0.5	3
KCl	3.2–66.5	4.6–95.0	3.2 ± 0.4	2.2 ± 0.3	3
NaBr	1.8	2.6	3.5 ± 0.8	2.5 ± 0.6	1
		Pulsed-Valve Experiments			
NaCl[d]		0.7–5.0		2.7 ± 0.5	7
KBr		1.5		3.5 ± 0.8	1
$NaNO_3$		5.0		3.5 ± 0.8	1
KCl		0.9–3.5		2.8 ± 0.5	2

[a] Number of molecules in the reactor at the start of the experiment. The density in molecules cm^{-3} is obtained by dividing by the cell volume (960 cm^3). [b] See text and eq 10. [c] k_{uni} is related to the uptake coefficient by the relation $k_{uni} = \omega\gamma$. For nitric acid at room temperature, $\omega = 90$ s^{-1}. [d] Average includes two small-orifice experiments; otherwise all experiments reported here are large-orifice results.

$$dN_i/dt = F - k_{esc}^{SV} N_i = 0 \quad \text{(before reaction)} \quad (6)$$

$$dN_f/dt = F - k_{uni} N_f - k_{esc}^{FV} N_f = 0 \quad \text{(during reaction)} \quad (7)$$

The symbol F represents the flow of HNO_3 into the cell (in molecule s^{-1}); N_i and N_f are the total number of HNO_3 molecules before and after the start of the experiment. Two different values of k_{esc} are needed because of the 30% volume change at the start of the experiment—the FV and SV superscripts refer to the small- or full-volume values. The mass spectrometer signal is proportional to the flux of nitric acid that enters the ionization volume; below, the symbol I is a constant to take this intensity proportionality into account. The signal before and after opening the sample chamber, S_i and S_f, can be expressed as follows:

$$S_i = I N_i k_{esc}^{SV} \quad (8)$$

$$S_f = I N_f k_{esc}^{FV} \quad (9)$$

The value for k_{uni} can be related to the ratio to the ratio of the initial and final steady-state signals by setting eq 6 equal to eq 7 and converting N into S with eqs 8 and 9:

$$k_{uni} = \left(\frac{S_i}{S_f} - 1\right) k_{esc}^{FV} \quad (10)$$

Application of eq 10 is the simplest possible treatment of the experimental data and includes the assumption that there is no saturation of the available surface sites during HNO_3 uptake. In addition, this treatment is only applicable to those experiments for which a steady-state uptake of HNO_3 is observed after the opening of the sample chamber. The validity of this simple analysis is supported by our observation that, for the chlorides studied, the ratio S_i/S_f remains constant over a large range of HNO_3 flow (cf. Table 2 and Figure 8). The value of k_{esc} used in eq 10 is simply the mass-scaled gas-kinetic value calculated from the expression in Table 1. The ratio S_i/S_f is taken at least

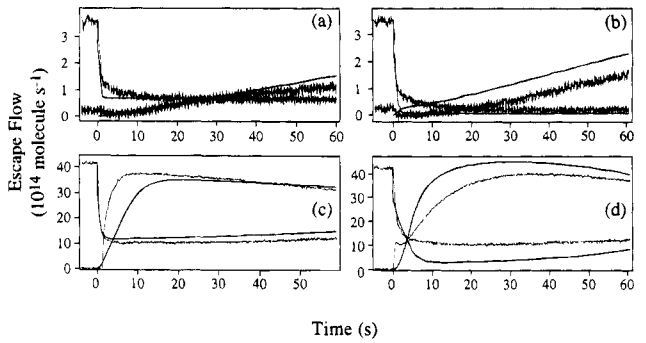

Figure 7. Set of steady-state experiments with systematically varied initial conditions: For (a) and (c), $k_{esc}^{HNO_3} = 0.7\ s^{-1}$; for (b) and (d), $k_{esc}^{HNO_3} = 0.1\ s^{-1}$. The lines that pass through or near the data are the results of the kinetics simulation presented in the discussion. Panels a and b represent low-flow experiments; (c) and (d) show high-flow results.

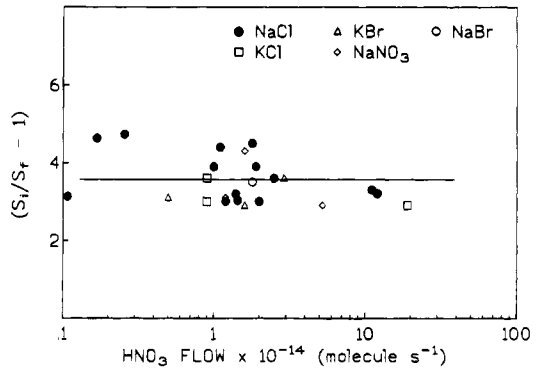

Figure 8. Plot of the observed "uptake" ($S_t/S_i - 1$) as a function HNO_3 flow for the large-aperture experiments for which a distant steady state was observed with respect to uptake of HNO_3 (see text and eq 10). Bromides are not included at higher flows because of a rapid saturation effect (cf. Figure 3).

10 s after the opening of the reaction to assure that the walls have reached steady state with respect to the new gas-phase density of HNO_3. The assumptions of this treatment are more rigorously justified in the next section by the application of a kinetic simulation.

In the above treatment, eq 10 has been applied only to the large-orifice experiments because, with a small orifice, the steady-state density of HNO_3 in the cell is an order of magnitude greater for the same inlet flow. With very small flows of HNO_3 (10^{12}–10^{13} molecules s^{-1}), small-orifice flow experiments can be analyzed by using eq 10 and the value of k_{uni} thus obtained is in good agreement with the large-orifice results given. An example of such an experiment is shown in Figure 9. At the flow rate used in this experiment (1.0×10^{13} molecules s^{-1}), an induction period for the formation of HCl is particularly apparent.

The results for experiments conducted on all salt samples in the low-exposure limit are presented in Table 2. Although the majority of the experiments were conducted by following the nitric acid concentration at the *m/e* 46 signal, a few were carried out with the same procedure using the *m/e* 63 signal; the latter is free of potential contributions due the presence of other oxides of nitrogen. The most striking aspect of the data summarized in Table 2 is the similarity in reactivity for all the salts studied; of particular note is that the nonreactive sample $NaNO_3$ is characterized by the same value of k_{uni} as the other samples. In Figure 8 we plot values of k_{uni} against the flow of nitric acid for the five salts studied with the large-aperture reactor. We note that for the three experiments of lowest HNO_3 density,

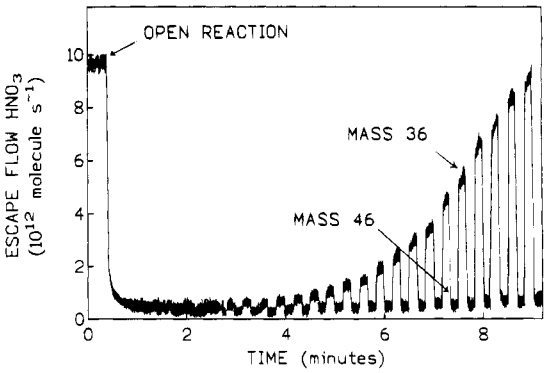

Figure 9. Result of a low-flow, small-orifice experiment ($k_{esc}^{HNO_3} = 0.1\ s^{-1}$). The HNO_3 density at the start of the experiment is 1.0×10^{11} molecules cm^{-3}. Note the long induction period for the production of HCl under these conditions.

the flow into the reactor was too small to be directly calibrated; the flow is estimated with the assumption that the mass-spectrometer response remains linear over the range of gas-phase densities studied. Steady-state uptake of HNO_3 is not observed on the bromide samples at the higher flow rates due to a more rapid onset of "saturation" and these experiments are not represented in the figure. Taking the average of all the low-dose steady-state experiments yields the value for k_{uni} of (2.4 ± 0.4) s^{-1} for the 10.8-cm^2 sample container employed. With the value of the collision frequency determined from the appropriate relation in Table 1, a value of $(2.8 \pm 0.3) \times 10^{-2}$ is calculated for the uptake coefficient.

The uptake of HNO_3 is the low-dose exposures does not depend on the milling conditions used to prepare the sample. The powders are occassionally analyzed by scanning electron microscopy, and it has been found that slight alterations of the milling procedure (such as degree of filling) have a dramatic effect on the resulting typical grain size. Some variation in k_{uni} is evident in Figure 8, but the rate of initial uptake does not vary systematically with the characteristic grain size of the salt powder, even if the longer time-scale behavior (i.e., onset of saturation) is influenced by this parameter.

D. Other Experiments. In this section are grouped together the results of several series of experiments designed to gain qualitative insight into the reactivity of the HNO_3–salt system; several of these are related to the determination of parameters for a kinetic simulation of the adsorption process that is described in the Discussion.

D.1. Systematic Variation of Initial Adsorption. In order to obtain a data set with which the kinetic model developed in the Discussion can be tested, experiments were performed with a variety of initial conditions (aperture size and HNO_3 flow) to observe the effect of varying nitric acid densities and residence time on the uptake kinetics. In particular, the experiments conducted at large flows (up to 1×10^{16} molecules s^{-1}) and with a small aperture ($k_{esc}^{HNO_3} = 0.10\ s^{-1}$) resulted in nitric acid exposures that rapidly exhausted the chemical potential of the salt sample. The long-term behavior is expected to be a function of the total internal surface area of the powder and of additional factors that are not easily controlled or characterized in a systematic fashion in these experiments. Thus, for this study, we limit the modeling to the first few tens of seconds of nitric-acid exposure. The goal of the modeling is to reproduce the magnitude of the HNO_3 uptake and the rate of the HCl appearance as a function of the experimental parameters varied. A set of four experiments is shown in Figure 7 for NaCl. The lines that pass through (or near) the data are the results of a kinetic simulation that is described in the Discussion.

D.2. Nitric Acid Desorption. In the limit of low exposure, we observe that the rate of HNO_3 uptake on $NaNO_3$ is the same as for the other salts studied (cf. Figure 4). However, the uptake in this case is nonreactive, and a rapid saturation of HNO_3 uptake is observed. When the sample is treated to complete saturation of its exposed and internal surfaces (S_{surf} and S_{HNO_3} in the model described below), and if the flow of nitric acid is turned off, the initial rate of desorption can be estimated by fitting an appropriate function to the experimental trace. An example of this type of experiment is shown in Figure 6, along with a control experiment showing the escape of nitric acid from the cell under identical conditions (no $NaNO_3$ present). Assuming that there is an additional source (D) from the sample outgassing and that the source is initially constant, we can modify $f_s(t)$ of eqs 2 and 3 to include the constant term:

$$f_s(t) = S_w e^{-(k_w t)} + D \tag{11}$$

Upon integration of eq 1 using this $f_s(t)$, eq 12 is derived:

$$N(t) = \frac{S_w}{(k_{esc} - k_w)} e^{-(k_w t)} + \frac{D}{k_{esc}} + \left(\frac{-S_w}{(k_{esc} - k_w)} + \frac{F_{int} - D}{k_{esc}} \right) e^{-(k_{esc} t)} \tag{12}$$

The parameters S_w and k_w are derived in a control experiment, as described above (cf. Figure 6, trace b). An experiment conducted with a desorbing solid sample (Figure 6, trace c), is analyzed by optimizing eq 12 to the experimental trace allowing only the constant D to vary. In this manner, the net production of HNO_3 from the degassing solid can be estimated for the first few seconds following the stopping of the inlet flow. From the experiment shown in Figure 6, we calculate this source of desorbing HNO_3 to be 7.0×10^{14} molecules s^{-1}. The implications of the result are discussed in the next section.

In a related experiment, the mass spectrum of the desorbing gas is recorded every 30 s for 10 min to see if a degradation of nitric acid can be observed on the nitrate samples. A degradation process, in particular resulting in the formation of NO_2, is a potential second reactive channel for the nitric acid interaction with the salt. As discussed above, we follow the *m/e* 46 peak to monitor nitric acid concentrations in the cell; thus, the presence of HNO_3 degradation could bias the conclusions concerning the uptake of the HNO_3. We find that the relative intensities of the *m/e* 30, 46, and 63 peaks remain constant during the admission, adsorption, and outgassing of HNO_3 from the nitrate sample. Under the present experimental conditions, there is no observable decomposition of HNO_3 on the Teflon-coated reactor walls, nor on the nonreactive $NaNO_3$ powder.

D.3. Dependence on Sample Presentation. If we increase the mass of the sample, conserving the same total exposed surface area, we find that (1) the rate of initial adsorption of HNO_3 remains unchanged but that (2) the saturation behavior (i.e., the time to bring about an onset of saturation and the time to achieve the maximum in the HCl production curve as observable in Figure 2) scales with the total mass of the sample. In three experiments, the geometric surface area of the sample was reduced by a factor of 2; the initial rate of uptake decreased by the same factor.

D.4. The Role of Humidity. In a low-pressure reactor, we have only limited means of characterizing the kinetics of HNO_3 uptake as a function of humidity. In a first experiment, a steady-state uptake of nitric acid was established under low-dose conditions, much like the steady state shown in Figure 7a. Then water vapor was added to the cell via the pulsed valve, each pulse containing about 1×10^{15} molecules of H_2O; no changes were observed in the steady-state process (rates of HNO_3 uptake and HCl production) due to the presence of water vapor. In a second experiment, water was added in a pulsed valve experiment in the absence of nitric acid. The results of this experiment are presented in Figure 10, where it can be seen that the loss of the H_2O in the presence of the NaCl sample is governed by the escape rate of the Knudsen cell. By analyzing experiments like that shown in Figure 10, we determine an upper limit for the uptake efficient, $\gamma < 2 \times 10^{-4}$, for the adsorption of H_2O on NaCl under our experimental conditions. Gas-phase water does not interact with the powder samples, and the presence of water does not play a role in the adsorption kinetics of nitric acid on NaCl over the limited range of humidity we are able to study by using the low-pressure reactor.

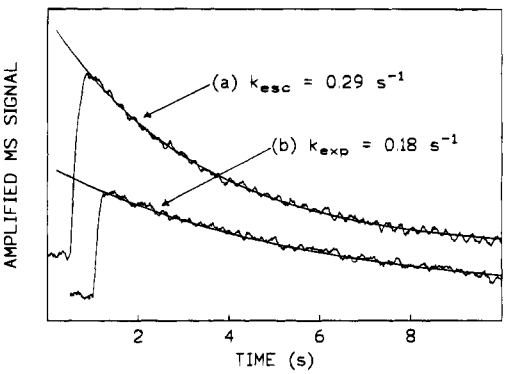

Figure 10. Real-time signal at *m/e* 18 (lock-in amplified) after pulsed injection of H_2O (small aperture): (a) Control experiment (NaCl powder isolated); (b) NaCl exposed. The rate of loss in both cases is governed by the escape rate of H_2O from the low-pressure reactor (the difference in rates is due to the volume change associated with the sample chamber). The baseline has been shifted for clarity.

D.5. HCl Uptake by NaCl. In control experiments, we established that HCl is efficiently adsorbed onto sodium chloride powder. The experiments were conducted in the reactor configured with the large aperture ($k_{esc}^{HCl} = 0.9$ s^{-1}) by using the steady-state procedure and employing low flows of HCl (5×10^{14} molecules s^{-1}); when the sample chamber is opened, a rapid drop of the HCl density is observed. With the simple steady-state analysis described above, we estimate the uptake coefficient for HCl adsorption on NaCl to be 3×10^{-2}. In addition, we have determined the total amount of HCl that can be adsorbed onto the sample to be 4.0×10^{16} molecules per gram of NaCl powder present. This latter parameter is dependent on the milling conditions of the sample, and is used as a guideline for the model developed in the Discussion. In a related experiment, it is found that HCl adsorbed onto NaCl is efficiently displaced by nitric acid. In Figure 11, it can be seen that when HCl-doped samples are exposed to HNO_3 in a low-flow steady-state experiment, a rapid rise in the HCl signal is seen, in stark contrast to the situation shown in Figure 7a, where a fresh sample is exposed to nitric acid under the same conditions. This suggests that HCl accumulates in the sample before it is seen as a product in the gas phase and that the release of HCl can be accelerated via a displacement reaction with nitric acid. In addition, the presence of HCl in the powder does not inhibit the uptake of HNO_3.

D.6. Uptake of HNO_3 at 70 °C. A small number of experiments have been conducted with a heated reactor ($T = 355$ K) to explore the temperature dependences of the HNO_3 adsorption on NaCl powder and the affinity of the HNO_3 for the reactor walls. From the expression given in Table 1, it can be calculated that raising the temperature to 355 K for room temperature results in a 10% increase in the value of k_{esc}.

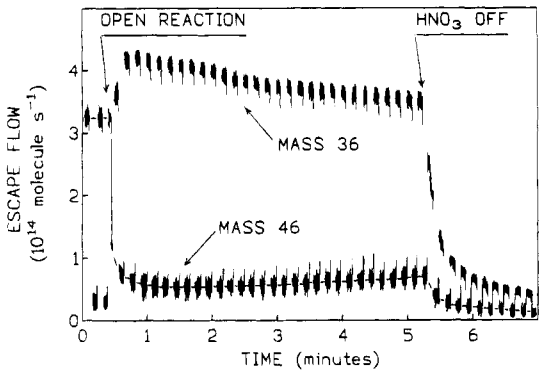

Figure 11. Experimental trace of a low-flow exposure (large orifice) of HNO_3 onto a NaCl sample previously exposed to HCl. The rapid rise of HCl at the start of the experiment can be compared to Figure 7a, conducted under comparable conditions. The displacement of the adsorbed HCl by HNO_3 holds implications for the model developed in the Discussion. Dashes have been added between the *m/e* 46 data points for clarity.

Analysis of a single steady-state experiment (large orifice, flow of $HNO_3 = 4.0 \times 10^{14}$ molecule s^{-1}) yields a value of 2.6 s^{-1} for k_{uni}, i.e., unchanged relative to the room-temperature rate. The value of k_{esc} measured at 355 K by using pulsed-valve injection of HNO_3 agrees with the calculated value based on the molecular mass of HNO_3 and the temperature. This supports the hypothesis that wall affinity of HNO_3 is responsible for the anomalous escape-rate behavior at room temperature.

Discussion

A rapid uptake of HNO_3 was observed for all the salt samples studied; in the limit of low doses, the two experimental techniques agree well, and we report the average of all determinations of the uptake coefficient: $\gamma = (2.8 \pm 0.3) \times 10^{-2}$. This value is independent of the total mass, temperature, and grain size of the powder sample. The rate of uptake remains constant over three orders of magnitude of HNO_3 flow (and thus on the gas-phase density). The good agreement between the two low-dose techniques is important because of the presence of wall effects. Both the nature of the wall-adsorption interference and the manner with which it is taken into account are specific to each technique. The consistency of the two data sets provides confidence that the procedures used to analyze the data are valid.

The rise of the HBr signal is shifted to longer times relative to the HCl signals observed for equivalently prepared bromide and chloride samples; also, the bromides saturate more readily than the chlorides. It is interesting to note that the thermochemistry of the displacement reactions (given in the Introduction) are more favorable for the chlorides. The kinetic model developed below for the case of the NaCl reaction may also be adapted for the bromides; more detailed experiments and analysis on bromide reactivity may be pursued in the future.

The remainder of our important experimental observations can be summarized in the following points: (1) The reactive uptake, k_{uni}, is proportional to the external surface area of the salt sample, and at higher doses the onset of uptake saturation is found to be a function of the sample's total mass. (2) The uptake rate of HNO_3 on $NaNO_3$ powder, for which no chemical interaction is observed, is the same as for the other salts studied. We quantify the rate of HNO_3 desorption from a saturated $NaNO_3$ powder. (3) There is no observable decomposition of nitric acid under the present experimental conditions. (4) HCl is adsorbed readily and reversibly to the NaCl powders and is rapidly displaced by nitric acid. (5) Water (at millitorr pressures) is not adsorbed onto the salt powder and its presence does not perturb the uptake of HNO_3 under these experimental conditions. (6) The rate of uptake in the low-dose limit does not vary as a function of temperature between 295 and 353 K.

TABLE 3: Units and Parameter Values Used in Kinetic Simulations

variable	units[a]	parameter	value[a]
$[HNO_3](g)$	cm^{-3}	k_1	3.0×10^{-14} cm^2 s^{-1}
$[HNO_3](phys)$	cm^{-2}	k_{-1}	1.1×10^{-2} cm^{-1} s^{-1}
$[HNO_3](int)$	g^{-1}	k_2	2.2×10^{-19} g cm^{-1} s^{-1}
[HCl](phys)	g^{-1}	k_3	1.1×10^{-19} g^2 cm^{-3} s^{-1}
[HCl](g)	cm^{-3}	k_4	2.2×10^{-19} g^2 cm^{-3} s^{-1}
S_{surf}	cm^{-2}	$S_{surf}(t=0)$	1.0×10^{14} g cm^{-2}
S_{HNO_3}	g^{-1}	$S_{HNO_3}(t=0)$	1.0×10^{18} g^{-1}
S_{HCl}	g^{-1}	$S_{HCl}(t=0)$	4.0×10^{16} g^{-1}

[a] The unit system is based on the density units (molecule cm^{-3}) commonly applied in gas-phase kinetics, so that the rate of change of a concentration is always expressed as molecule cm^{-3} s^{-1}, even if the species is physisorbed on the solid phase.

The experimental observations are unified with a kinetic model of HNO_3 uptake on NaCl. A similar approach has been taken recently to describe the uptake of NO_2 on amorphous carbon samples.[31] We want to reproduce the time dependence of the HNO_3 uptake and the rate of HCl formation as a function of the nitric acid flow. In particular, at low flows of nitric acid, there appears to be an "induction period" between the beginning of the exposure and the formation of gas-phase HCl (cf. Figures 7 and 9). The two hypotheses that can be posed for this observation are that (1) the HNO_3 adsorbed onto the surface exists in a nonreactive intermediate state before reacting and/or that (2) the reaction leading to HCl formation is rapid and the HCl product must pass through a bound state with the salt before release into the gas phase. Based on the results of our HCl uptake experiments, we infer that the latter plays an important role. The model applied to the kinetic experiments is a four-step process, including surface adsorption and desorption (k_1 and k_{-1}), communication of adsorbed HNO_3 with the bulk solid (k_2 and k_{-2}), and subsequent reaction (k_3) and liberation (k_4) of the HCl product. Below, the sequence is written for the reaction of nitric acid with a chloride:

reaction	parameters
$HNO_3(g) + S_{surf} \rightleftharpoons HNO_3(phys)$	k_1, k_{-1}, S_{surf}
$HNO_3(phys) + S_{HNO_3} \rightleftharpoons HNO_3(int) + S_{surf}$	k_2, k_{-2}, S_{HNO_3}
$HNO_3(int) + S_{HCl} \rightarrow HCl(int)$	k_3, S_{HCl}
$HNO_3(int) + HCl(int) \rightarrow HCl(g) + HNO_3(int) + S_{HCl}$	k_4

In this scheme, S_{surf}, S_{HNO_3}, and S_{HCl} represent the number of surface sites, internal reactive sites for HNO_3, and the reservoir size for HCl, respectively. The qualifiers represent the gaseous state (g), a surface physisorbed state (phys), and a physisorbed state in the bulk (int).

As much as possible, the values for the modeling are determined or constrained by the experimental observations. The constant k_1 is taken from the rate of uptake determined from the low-dose experiments. The constant k_{-1} can be estimated from the initial rate of HNO_3 desorption from $NaNO_3$ powder. The following assumptions are made: (1) $NaNO_3$ has the same desorption properties as NaCl and (2) the initial rate of desorption, which is given by the product $k_{-1}[HNO_3](phys)$ in the above model, can be approximated by $k_{-1}S_{surf}$ (i.e., initially, all the available surface sites for HNO_3 adsorption are occupied). With the values from Table 3, k_{-1} is estimated to be 0.7 s^{-1}. The model is insensitive to k_{-1} for all values less than or equal to this estimated value (because k_2 is large; cf. footnote of Table 3). The interesting observation that HNO_3 is initially taken up on $NaNO_3$ with the same efficiency as the other salts studied is

TABLE 4

A. Comparison with Previous work

oxide	substrate	uptake coeff	notes
NO_2	Syn. Seasalt	$10^{-6}-10^{-7}$	flow reactor, ref 8
NO_2	NaCl	"rapid"	bulk measurement, ref 10
NO_2	Wet NaCl	$<10^{-4}$	smog chamber, ref 12
NO_2	NaCl	$>5 \times 10^{-8}$	bulk measurement, ref 9
N_2O_5	NaCl	>0.025	bulk measurement, ref 13
N_2O_5	wet NaCl	0.032 ± 0.003	smog chamber, ref 14
HNO_3	wet NaCl	rapid	aerosol reactor, ref 15
HNO_3	various salts	0.028	low-pressure reactor, this work

B. Typical Atmospheric Densities

oxide	remote atmosphere[a]	polluted atmosphere[b]
NO_2	4.8 pptv	100–800 ppbv
HNO_3	16 pptv	50 ppb
N_2O_5[c]	1 ppt	1 ppb

[a] Values taken from ref 33 for the equatorial Pacific. [b] Values taken from ref 1. [c] Values estimated in ref 34.

strong evidence for the formation of the intermediate species HNO_3(phys) and HNO_3(int). The second step, which models the HNO_3 communication with the bulk of the powder sample, is introduced to describe the sample-mass dependence of the long-term or high-exposure saturation behavior. The existence of a HCl(int) species and a displacement reaction between it and HNO_3(int) are supported by the experiments that characterized the HCl uptake and its displacement by HNO_3 on NaCl powders. Finally, the magnitudes of the parameters S_{HNO_3} and S_{HCl} are determined experimentally by integrating the number of molecules required to completely saturate a nonreactive substrate (HNO_3 on $NaNO_3$, HCl on NaCl).

In Figure 7, we show how the model reproduces a data set selected to represent a range of initial conditions. The parameters used for the modeling are given in Table 3. In general, the agreement between the simulation and experiments is good, particularly when the simplicity of the model is considered. The inclusion of other processes would certainly improve the agreement between the simulation and experiment. Since we have no technique to observe directly the physisorbed species on the surface or in the bulk of the salt powders, we prefer the simplest mechanism that can (a) reproduce the features of the experiments and (b) account for the ensemble of observations outlined at the beginning of the Discussion. The most significant conclusion is that the rate constant of HNO_3 uptake is, within this model, consistent with the results of a series of experiments conducted under different initial conditions, and thus the model can be used to predict the reactivity of gaseous nitric acid with respect to salt over several decades of gas-phase concentration. One notable feature of Figure 7 is the slow approach to the steady state for the small flow experiments (panels a and b); the time scale for this process is on the order of 10 s, comparable to the rate of wall degassing determined in section B of the Results. In the model, the appearance of the HCl is governed by a bimolecular process—reaction R-3 in the above scheme. The bimolecular displacement reaction between physisorbed species is reasonably successful in reproducing the rate of HCl formation over the range of initial conditions employed.

The nitric acid densities attained in this study are comparable to those observed in the atmosphere; in the lowest flow experiments, the initial density (before start of experiment) in the cell is on the order of 10^{10} molecules cm^{-3}, corresponding to the ppbv level appropriate to the atmosphere (cf. Table 4). The other aspects of the experimental configuration represent less well the atmospheric chemical environment. Most notably, the powders of pure alkali salts may not reflect the reactivity of sea-salt aerosols. Also, gas-phase water does not interact with the salt powders under the experimental conditions employed. The lack of water uptake onto at low partial pressures of H_2O is a phenomenon that has been observed previously for salt aerosols.[32] The process becomes efficient when the relative humidity approaches the deliquescence point of the salt; these humidities are not attainable with our low-pressure reactor. It is, however, interesting to note that values for γ that are derived from direct gas–solid contact are often in good agreement with values determined with smog chambers, with which the effects of humidity can be tested (cf. Table 4). Indeed, our experimental results provide strong evidence that HNO_3 reacts efficiently with salt-containing aerosols to form HCl or HBr, as proposed previously by a number of authors. In Table 4, we compare the value of γ obtained in this work for the HNO_3 adsorption on NaCl to those obtained previously for the uptake of NO_2 and N_2O_5 on the same salt. Atmospheric concentrations of HNO_3, N_2O_5, and NO_2 have been measured or inferred in many studies, and for sake of comparison we quote the values measured recently in the equatorial pacific troposphere to represent "remote" conditions.[33] At nighttime, there is formation of N_2O_5, and the concentration in the remote marine environment may reach a few ppt.[34] For the typical tropospheric concentrations of these three oxides of nitrogen, reaction R-1 may be responsible for the largest fraction of chloride displacement in marine aerosols. Since the data on N_2O_5 and NO_2 reactivity have been acquired mostly by crude bulk measurements and by smog-chamber measurements, the assessment of the relative contributions of the nitrogen oxides to chloride displacement is still extremely uncertain. We are currently in the process of studying the NO_2 and N_2O_5 uptake by salt samples to establish a coherent set of kinetic data that will shed additional light on the reaction mechanisms and on the relative reactivities of these nitrogen oxides with respect to uptake on salt.

Our observation that the salt samples have an affinity to reversibly and efficiently adsorb small amounts of HCl may be relevant to the discussion of marine aerosol reactivity; it suggests that secondary surface reactions between the adsorbed HCl and atmospheric gas-phase species may be possible. In recent work by Keene and co-workers,[3,5] it has been proposed that a cyclic processing of gaseous chlorine species by aerosols may increase significantly the chlorine atom concentration in the marine troposphere; one of the steps in their proposed mechanism is the efficient ($\gamma = 0.15$) uptake of HCl by the sea-salt aerosols. In smog-chamber studies by Behnke et al., it was reported that the reactivity of N_2O_5 increases, with respect to pure NaCl, when exposed to an aerosol generated from an authentic sample of sea salt.[12,14] In addition, they report that ozone may be capable of generating chlorine atom precursors by reaction with sea-salt aerosol.[14] It is possible that secondary reactions involving adsorbed HCl with gas-phase species are contributing to the enhanced reactivity.

Summary

We have derived for the first time an uptake coefficient for the atmospherically important interaction between nitric acid and salt. The sole product of the reaction, HCl (or HBr), is produced in 100% yield. In addition, we found that HCl can exist in a physisorbed state on NaCl powder. A simple, empirically derived model is able to reproduce the observations of the NaCl–HNO_3 interaction over a broad range of experimental conditions. With the newly determined value of γ, we conclude that HNO_3 may be responsible for most of the chloride displacement from sea-salt aerosol.

Acknowledgment. Funding for this work was provided by the Office Fédéral de l'Education et de la Science (OFES) under Grant 581.352 as part of the HALIPP subproject of the EUROTRAC program. We thank Hubert van den Bergh for his lively interest and input.

References and Notes

(1) Finlayson-Pitts, B. J.; Pitts, J. N. *Atmospheric Chemistry*; John Wiley and Sons: New York, 1986.

(2) Singh, H. B.; Kasting, J. F. *J. Atmos. Chem.* **1988**, *7*, 261.

(3) Keene, W. C.; Pszenny, A. A. P.; Jacob, D. J.; Duce, R. A.; Galloway, J. N.; Schultz-Tokos, J. J.; Sievering, H.; Boatman, J. F. *Global Biogeochem. Cycles* **1990**, *4*, 407.

(4) Chameides, W. L.; Stelson, A. W. *J. Geophys. Res.* **1992**, *97* (D18), 20565.

(5) Pszenny, A. A. P.; Keene, W. C.; Jacob, D. J.; Fan, S.; Maben, J. R.; Zetwo, M. P.; Springer-Young, M.; Galloway, J. N. *Geophys. Res. Lett.* **1993**, *8*, 699.

(6) Finlayson-Pitts, B. J. *J. Geophys. Res.* **1993**, *98* (D8), 14991.

(7) Parrish, D. D.; Hahn, C. J.; Williams, E. J.; Norton, R. B.; Fehsenfeld, F. C.; Singh, H. B.; Shetter, J. D.; Gandrud, B. W.; Ridley, B. A. *J. Geophys. Res.* **1993**, *98* (D8), 14995.

(8) Sverdrup, G. M.; Kuhlman, M. R. *Atmos. Pollution 1980*; Proceedings of the 14th International Colloquium, Paris, France, 1980; Vol. 8, p 245.

(9) Finlayson-Pitts, B. J. *Nature* **1983**, *306*, 676.

(10) Schroeder, W. H.; Urone, P. *Environ. Sci. Technol.* **1974**, *8*, 765.

(11) Winkler, T.; Goschnick, J.; Ache, H. J. *J. Aerosol Sci.* **1991**, *22* (Suppl. 1), S605.

(12) Behnke, W.; Krueger, H.-U.; Scheer, V.; Zetzsch, C. *Proceedings of the EUROTRAC Symposium '92*; Borrell, P. M., Ed.; SPB Academic Publishing; The Hague, The Netherlands, 1993.

(13) Livingston, F. E.; Finlayson-Pitts, B. J. *Geophys. Res. Lett.* **1991**, *18*, 17.

(14) Behnke, W.; Krueger, H.-J.; Scheer, V.; Zetzsch, C. *J. Aersol. Sci.* **1992**, *23* (Suppl. 1), S933.

(15) Cadle, R. D.; Robbins, R. C. *Discuss. Faraday Soc.* **1960**, *30*, 155.

(16) Green, W. D. *J. Geophys. Res.* **1972**, *77*, 5152.

(17) Martens, C. S.; Wesolowski, J. J.; Harriss, R. C.; Kaifer, R. *J. Geophys. Res.* **1973**, *78*, 8778.

(18) Clegg, S. L.; Brimblecombe, P. *Atmos. Environ.* **1985**, *19*, 465.

(19) Brimblecombe, P.; Clegg, S. L. *J. Atmos. Chem.* **1988**, *7*, 1.

(20) Mamane, Y.; Mehler, M. *Atmos. Environ.* **1987**, *9*, 1989.

(21) Mamane, Y.; Gottlieb, J. *J. Aersol. Sci.* **1990**, *21* (Suppl. 1), S225.

(22) Dasch, J. M.; Cadle, S. H. *Atmos. Environ.* **1990**, *24A*, 2557.

(23) Mamane, Y.; Gottlieb, J. *Atmos. Environ.* **1992**, *26A*, 1763.

(24) Hidy, G. M.; Mueller, P. K.; Wang, H. H.; Karney, J.; Twiss, S.; Imada, M.; Alcocer, A. *J. Appl. Meteor.* **1974**, *13*, 96.

(25) Kobayashi, T.; Ikezawa, T.; Watanabe, H. *Taiki Osen Gakkaishi*, **1979**, *14*, 401.

(26) Michelangeli, D. V.; Allen, M.; Yung, Y. L. *Geophys. Res. Lett.* **1991**, *18*, 673.

(27) Golden, D. M.; Spokes, G. N.; Benson, S. W. *Angew. Chem., Int. Ed.* **1973**, *12*, 534.

(28) Müller-Markgraf, W.; Rossi, M. J. *Rev. Sci. Instrum.* **1990**, *61*, 1217.

(29) Svensson, R.; Ljungstroem, E.; Lindqvist, O. *Atmos. Environ.* **1987**, *21*, 1529.

(30) Pitts, J. N., Jr.; Sanhueza, E.; Atkinson, R.; Carter, W. P. L.; Winer, A. M.; Harris, G. W.; Plum, C. N. *Int. J. Chem. Kin.* **1984**, *16*, 919.

(31) Tabor, K.; Gutzwiller, L.; Rossi, M. J. *J. Phys. Chem.* **1994**, *98*, 6172.

(32) Svenningson, I. B.; Hansson, H.-C.; Wiedensohler, A. *Tellus* **1992**, *44B*, 556 and the references cited therein.

(33) Torres, A. L.; Thompson, A. M. *J. Geophys. Res.* **1993**, *98* (D9), 16949.

(34) Ganske, J. A.; Berko, H. N.; Finlayson-Pitts, B. J. *J. Geophys. Res.* **1992**, *97* (D7), 7651.